Bollettino di Geofisica Teorica ed Applicata Vol. 53, n. 1, pp. 169-190; March 2012
DOI 10.4430/bgta0039

Pre-seismic phenomena from continuous near-field strain measurements: a brief review and the case of the 2009 L'Aquila, Italy, earthquake

A. Amoruso and L. Crescentini

Dipartimento di Fisica, Università di Salerno, Fisciano, Italy

(Received: June 6, 2010; accepted: November 17, 2010)

ABSTRACT After a brief (incomplete) review of pre-seismic (strain-producing) phenomena, we describe our findings about the pre-seismic phase of the the April 6, 2009 L'Aquila earthquake, giving a few more details with respect to previous papers. Most past observations of crustal strain did not detect any pre-seismic deformation and have been used to constrain the size and strength of the source of possible pre-seismic phenomena. With respect to these, we performed a rather more sophisticated approach to the physics of the model; limited the volume of the possible earthquake preparation zone to less than 100 km^3; showed some evidence of dilatancy of saturated rock over the earthquake causative fault (maybe related to the foreshocks) and constrained the prerupture nucleation slip in the hypocentral region to a moment less than 0.00005% of the main shock seismic moment (lowering the previous thresholds).

Key words: L'Aquila earthquake, strain measurements, earthquake prediction.

1. Brief review of pre-seismic phenomena (mainly) from continuos near-field strain measurements

1.1. Basics

Earthquake prediction is a difficult but stimulating challenge for the scientific community. The very meaning of the words "earthquake prediction" have to be clarified in terms of warning time, scientific bases, feasibility and mitigation measures [for a review, see e.g., Scholz (2002)], and the feasibility is unknown or fair for short- and intermediate-term predictions.

However, many claims of successful earthquake predictions are present in the literature. Among the phenomena proposed as precursors, strain-rate changes, changes in seismic wave velocities, electromagnetic signals, radon anomalies [for a review, see e.g., Kanamori (2003)] are included. Here, we briefly report on strain-related phenomena only, trying to put light on their relation with detectable strain for the final sake of comparison with our (strain) measurements. We start with a short remark about the most popular, at least in the case of the April 6, 2009 L'Aquila earthquake, precursor phenomenon, i. e., the radon anomalies. In the months before and after the main shock, plenty of events were "predicted" by using radon measurements (Giuliani *et al*., 2009), and after the occurrence of the April 6 L'Aquila earthquake it was rumored that the main shock had been preceded by radon anomalies clearly predicting it (Giuliani *et al*., 2009). Still now, the general public asks for information relating to radon measurements in the L'Aquila area, and elsewhere too. Even in the recent past, pre-seismic radon anomalies were often justified

as a large scale phenomenon in the frame of the resulting relations between earthquake magnitude and distance from the epicenter defining where the pre-seismic effects should be detectable (e.g., Einarsson *et al*., 2008; Ghosh *et al*., 2009; Singh *et al*., 2009). Radon anomalies are generally ascribed to the development of micro-cracks, fissures and fractures due to the dilatancy of rock over large regions prior to earthquakes. The presence of a dilatant zone would constitute an inhomogeneity in an otherwise undisturbed medium, perturb an applied tectonic stress field which is uniform at large distances and produce a strain disturbance potentially detectable by close strain meters. Further diagnostics of large-scale changes in physical properties of rock should come from possible changes in tidal shear strain and volumetric strain response, before or as a result of an earthquake (Nishimura, 1950). By the way, quantification of possible pre-seismic temporal changes of material properties in the near-surface layers would lead to a better characterization of site response, and accurate predictions of strong ground motions in the event of an earthquake.

In the meantime, detectable precursory strain could also be associated to phenomena related to the "local" earthquake nucleation phase, and pre-seismic crustal deformation can also potentially discriminate between theories of the earthquake generation process.

From the general point of view of fault mechanics, the physical bases of precursory phenomena rely either on fault or on bulk rock constitutive relations, which do or do not predict physical property changes respectively, and give rise to different models among which dilatancy models (Nur, 1972; Scholz *et al*., 1973) and nucleation ones are prominent [for a review, see e.g., Scholz (2002)].

As regards dilatancy models, they can be divided into two classes: volume dilatancy models and fault zone dilatancy models, that assume that dilatancy occurs in a volume of rock surrounding the fault zone or only within the fault zone itself. The most famous model is the dilatancy-diffusion one (Nur, 1972; Scholz *et al*., 1973), belonging to the volume-dilatancy family, that predicts many different types of precursory phenomena (changes in V_P/V_S, electrical resistivity, rate flow of water or radon emission, vertical motion, tilt and volumetric strain, number of seismic events) and a scaling relationship between the duration of the precursors and the volume of the dilatant region, and thus the magnitude of the earthquake, provided the dilatant volume is proportional to the magnitude of the event. In the fault zone dilatancy models, dilatancy occurs within the fault zone, just as slip occurs during nucleation, and is assumed to be proportional to slip. Therefore, there is an increase of the stiffness of the medium from the drained to the undrained modulus as dilatancy reduces the pore pressure within the fault zone, and a dilatancy hardening of the fault occurs (producing an increase in frictional resistance). Thus, the fault will be temporarily stabilized and the nucleation process will be effective after some time delay related to the hydraulic diffusivity of the fault zone. Precursory strain changes have been estimated from numerical simulations (Rice and Rudnicki, 1979) of a spherical 1-km radius "inclusion" of strain weakening material embedded in an elastic medium, under steadily increasing tectonic stress. Precursory strain could be detectable in the phase of rapid acceleration of strain near instability, since surface strain will have a time history similar to that of the inclusion strain even if attenuated. According to Rice and Rudnicki (1979), the most appropriate period in searching for precursory strain would be approximately 2 to 10 days for a spherical zone of a 1-km radius, and a much shorter one for a flattened ellipsoid. Larger zones would lead to longer precursor times.

As regards nucleation models, the basic assumption is that instability will not occur until slip has occurred over a fault patch of critical size. The fault patch will grow to reach the critical size, during the nucleation time, and the size is function of the fault strength, state of stress, and elastic constants of the surrounding rock. The nucleation process could be detectable by close strainmeters, giving it a sufficiently large nucleation zone and slip.

Laboratory studies and numerical simulations suggest that fault failure is preceded by subsonic pre-seismic slip (Dieterich and Kilgore, 1996; Lockner, 1998). Numerical simulations of earthquake nucleation on rate-and-state friction faults, under both "aging" and "slip" versions of the state evolution law indicate that "to the extent that laboratory evolution laws and rate-and-state parameters can be safely applied to the Earth" the nucleation zone should not exceed the order of 10 m (Ampuero and Rubin, 2008). The nucleation half-length scales with the characteristic sliding distance for the evolution of the state variable, which is ~ 10 μm from laboratory experiments, but might be as large as 10 mm in the seismogenic zone (Scholz, 1988). Also, heterogeneous initial conditions or normal stress may lead to nucleation zone expansion (e.g., Kaneko and Lapusta, 2008). More recently, it has been suggested (Fang *et al*., 2010) that moderate late-stage expansion of the nucleation zone may appear in the final moments of the nucleation process, usually 10 to 100 seconds (up to 10,000 seconds in extreme cases) prior to earthquake instability.

1.2. Observations

Many experimental data aiming to characterize possible different aspects of pre-seismic behavior and to interpret observations have been investigated.

As regards precursory strain changes, reports were made for earthquakes in both magmatic and nonmagmatic settings, but only a few reports are considered reliable evidence of pre-seismic changes (see e.g., Roeloffs, 2006). Pre-earthquake deformation-rate changes span a large time interval, lasting hundreds of seconds to more than a decade. In summary, most M>7.5 earthquakes occurred without detectable pre-earthquake deformation, and most observation of deformation rate changes are inconsistent with accelerating slip on the earthquake rupture plane, since they exhibit signs that are opposite to co-seismic changes, or a moment that exceeds the earthquake seismic moment.

Among the events producing detected pre-seismic deformation, the earthquake swarms related to volcanic activity off the east coast of the Izu peninsula (Japan, where at least four of these swarms have been preceded by strain rate changes) could be an example of deformation driven by magmatic processes, and the M 3.5 2002 Corinth Rift (Greece) earthquake could be an example of pre-seismic accelerating strain preceding a small event (Roeloffs, 2006). In particular, as regards the 1978 Izu-Oshima Kinkai earthquake (Inouchi and Sato, 1979), 15 cm of uplift had been observed between 1974 and 1976, near the western end of the rupture zone, moreover in the five years prior to the earthquake, a lengthening of 5-6 cm of the geodetic lines between the peninsula and Izu Oshima Island had been measured. All the observations are consistent with an expansion area north of the rupture (Roeloffs, 2006). As regards the case of the M 3.5 2002 Corinth Rift (Greece) earthquake (Bernard *et al*., 2004), even if other similar strain changes have been recorded without earthquakes, the steep rise time of the transient is quite different from the noise, but its decay is more similar to the noise (Roeloffs, 2006). Moreover, the decay of the

transient signal is inconsistent with unidirectional slips on a single fault plane, and could indicate fluid flow, propagation of the source, or activation of a secondary fault (Roeloffs, 2006). Among the events that have not produced detected pre-seismic deformation, the most popular is the 2004 Parkfield earthquake (see further on in the text for more details). Lack of pre-seismic observations, in the case of the M_w 6.0 2004 Parkfield earthquake and other events, have been used to constrain the size and strength of the pre-seismic phenomenon source (e.g., Wyatt *et al*., 1994; Abercombie *et al*., 1995; Johnston and Linde, 2002; Johnston *et al*., 2006). Examples of inconsistency with the hypothesis of noticeable stress built-up before an earthquake also come from the analyses of seismic velocities and anisotropy, as in the case of the *M* 6.4 Chia-Yi (Taiwan) 1999 earthquake (Chao and Peng, 2009), where the observed temporal changes of seismic velocity were mostly controlled by the variation of material properties in the top 200 m of the crust and the changes in the shear wave splitting delay time before the main shock did not appear statistically significant. However, the analysis of the foreshock sequence of the 1992 Landers, California, earthquake, suggested that foreshocks may have been driven by an aseismic creep over a kilometer-scale nucleation zone (Dodge *et al*., 1996). Moreover, two alternative interpretations of near-source observations of the seismic nucleation phase of several earthquakes (whose duration - for *M* 5.5 to 6.4 earthquakes- is tenths of a second, whose radius is hundreds of meters, and whose seismic moment is 10^{-4} to 10^{-2} of the mainshock seismic moment) have been given by Beroza and Ellsworth (1996), namely the pre-slip model and the cascade (or runaway) model. In the pre-slip interpretation, the seismic nucleation phase represents the very last stage of failure within the pre-slip zone before the propagation along the fault with large slip and high rupture velocity begins, and thus explains the duration of the seismic nucleation phase as the time required for the final rupture of the pre-slip zone. It is an alternative to the cascade (or runaway) interpretation, that explains the seismic nucleation as an accumulation of increasingly larger subevents: a large earthquake occurs when a smaller earthquake triggers a cascade of increasingly larger slip events. The two interpretations are both capable of explaining the observations in Beroza and Ellsworth (1996), but have quite different implications for earthquake prediction. In particular, the slip model would indicate a nucleation-zone size scaling with the size of the eventual earthquake.

As regards possible changes in tidal response, large changes have been reported several tens of km from the epicenter of a magnitude-6 earthquake (Zhang et al., 2002). In the same paper, the occurrence of abnormal deformation, similar to that observed before the Zhangbei (China) earthquake (M_s 6.2, occurred on January 10, 1998), is reported. The anomalous character of the observation was established according to a synthetic anomaly degree (SAD) value based on the analyses of long time series of many potentially precursor parameters trying to consider multiple-observation and their time, space and intensity characteristics. The SAD value of the Zhangiiakou, Huailai, and Yangyuan stations (epicentral distance are 60 km, 130 km and 110 km, respectively) were reported as being significant (Zhang *et al*., 2002), but mainly at the Zhangjiakou station, where almost all the different measurements and all the precursor parameters showed the anomaly. Months before the earthquake, tidal admittance amplitude changes reached 20% (4% being the claimed threshold value), thus suggesting a noticeable large-scale change in the elastic properties of the Earth's crust.

Large effects have rarely been observed. In (almost) all the cases investigated precursory

strain changes are small and it may be challenging to detect them: as an overall "comprehensive summary" of the efforts, we give a few details about the most famous attempt to reveal precursory behavior of different phenomena, i. e., the 2004 Parkfield, California, Earthquake (M_w 6.0). The instrumentation monitoring the Parkfield segment of the San Andreas fault was incremented in the late 1980s (monitoring system including water wells, high-resolution strain, electric field, magnetic field, and seismic-wave detectors) to catch possible precursors of the next event, in the frame of the Parkfield Earthquake Prediction Experiment. In fact, quite similar M 6 earthquakes occurred in the Parkfield area in 1857, 1881, 1901, 1922, 1934, and 1966, moreover it had been anticipated that another M 6 event would occur before 1993. No earthquake occurred before 1993, but a M 6 earthquake occurred on September 28, 2004. "Nothing unusual (statistically significant) was recorded before the mainshock" [e.g., references in Harris and Arrowsmith (2006)], and the suggestion was that "predicting the general timing and size of moderate and large earthquakes is difficult" and that "preselection of magnitude for the Parkfield earthquakes is what led to the apparently nonrandom recurrence statistics". However, many important results come from the Parkfield Earthquake Prediction Experiment. Among the most significant ones, the interseismic slip rate of the San Andreas Fault near Parkfield varied between the 1966 and the 2004 earthquakes (Roeloffs, 2006). For example, a higher slip rate was measured between 1992 and 1995 accompanied by a faster recurrence of repeating micro-earthquakes, and three $M > 4$ earthquakes also occurred near the 1966 Parkfield mainshock hypocenter during this period, but the fault slip rate subsequently returned to pre-anomaly values thus indicating that changes in inter-seismic deformation rates are not necessarily earthquake precursors. Moreover, the 2004 Parkfield earthquake had no foreshocks, contrary to the 1966 Parkfield earthquake, which was preceded by a foreshock and for which reports of pre-earthquake surface slip have been given. Another important result from the Parkfield Earthquake Prediction Experiment was that details of the slip distribution from the analysis of different types of observations (e.g., surface-slip measurements, InSAR, GPS, strong ground motion) differ, but distinct slip features consistent with all of the observations can be found. Focusing on crustal deformation, instrumentation at Parkfield included 12 creepmeters, a dual-frequency electronic distance meter (two-color EDM), eight dilatometers, and three three-component strainmeters in boreholes 170-320 m deep. Even if, by September 2004, three dilatometers and one three-component borehole strainmeter had ceased working, and the two-color EDM measurements were being made less frequently, the deformation data recorded before, during and after the 2004 Parkfield earthquake were more abundant and closer to the hypocenter of an M 6 earthquake than in any other previous case (Roeloffs, 2006). No significant changes in crustal deformation rates were detected in the weeks or minutes prior to the 2004 Parkfield earthquake. Borehole strainmeters (located about 15 km from the epicenter) and accelerometers (located immediately above the hypocenter) clearly demonstrated that in the last few seconds before the earthquake the maximum seismic moment release that could go undetected was less than 0.001% (as obtained from strain data, and 0.0001% from accelerometric data) of the earthquake seismic moment. The source size was also estimated, resulting in < 34 m using the strain data and < 12 m using displacement data (Johnston *et al*., 2006). As for other large magnitude earthquakes (Johnston and Linde, 2002) the scale on which rupture initiates seems to be several orders of magnitude smaller than that of the subsequent earthquake, thus indicating a nucleation runaway as the likely failure mechanism and conflicting

with suggestions (Beroza and Ellsworth, 1996) that nucleation scales with earthquake magnitude. The tidal response for the two years prior to the earthquake and after it have been determined (Johnston *et al*., 2006) by computing M2 tidal response as a function of time on either side of the rupture and at a distance of about 15 km from the epicenter. Differences have been constrained to less that 5%, thus suggesting no permanent changes, in agreement with results for other earthquakes (e.g., Linde *et al*., 1992).

As a conclusion of this brief review of pre-seismic phenomena (mainly) from continuous near-field strain measurements, "in many cases of purported precursory behavior, the reported observational data are contradictory and unsuitable for a rigorous statistical evaluation. One related problem is a bias towards publishing positive rather than negative results, so that the rate of false negatives (earthquake but no precursory signal) cannot be ascertained. A second is the frequent lack of baseline studies that establish noise levels in the observational time series." (International Commission on Earthquake Forecasting for Civil Protection, Operational Earthquake Forecasting: State of Knowledge and Guidelines for Utilization, Italian Civil Protection Department, 2009; http://www.protezionecivile.it/cms/attach/ex_sum_finale_eng1.pdf).

2. The case of the 2009 L'Aquila, Italy, earthquake

In the case of the 2009 L'Aquila earthquake, claimed earthquake precursors and preparation-phase-related phenomena include radon anomalies (Giuliani *et al*., 2009), radio anomalies (Biagi *et al*., 2009), space-time anomalies in thermal infra-red (TIR) satellite imagery (Lisi *et al*., 2010), and uranium groundwater anomalies (Plastino *et al*., 2010). Moreover, anomalies in the V_p/V_s ratio during the days preceding the main shock of April 6 have been reported by Di Luccio *et al*. (2010), i. e. a 5% increase of V_p/V_s along a path parallel to the NW-SE striking earthquake causative fault.

In the following paragraphs, after a brief technical description of the experimental apparatus, we show details of the analyses of strain data recorded before the M_w 6.3 April 6, 2009 L'Aquila earthquake by two crossed laser strainmeters operating in the Gran Sasso underground observatory, at a distance of about 20 km from the epicenter. Both the magnitude and the epicenter-instrument distance are similar to the Parkfield earthquake case. We performed (Amoruso and Crescentini, 2010) a rather more sophisticated approach to the physics of the model than in Johnston *et al*. (2006), and we significantly lowered the thresholds for the moment released before the earthquake and possible strain tidal changes. We also put a constraint on the relevant features (size and change in elastic parameter values) of a possible preparation zone. Besides illustrating some details of the results, not given in Amoruso and Crescentini (2010), we briefly discuss their relationships with claimed earthquake precursors and preparation-phase-related phenomena.

The two laser strainmeters (located about 1400 m underground, close to the LNGS-INFN Laboratori Nazionali del Gran Sasso - Istituto Nazionale di Fisica Nucleare laboratory, Fig. 1) measured the difference in extension between the two baselines (BA and BC, one about parallel to the local direction of the Apennines, and the other perpendicular to it) since 1995 and both independent extensions since 1999 (Crescentini *et al*., 1997; Amoruso and Crescentini, 2009a). In what follows, extensions are expressed as dimensionless strain, $\varepsilon = \Delta l/l$, where l is the

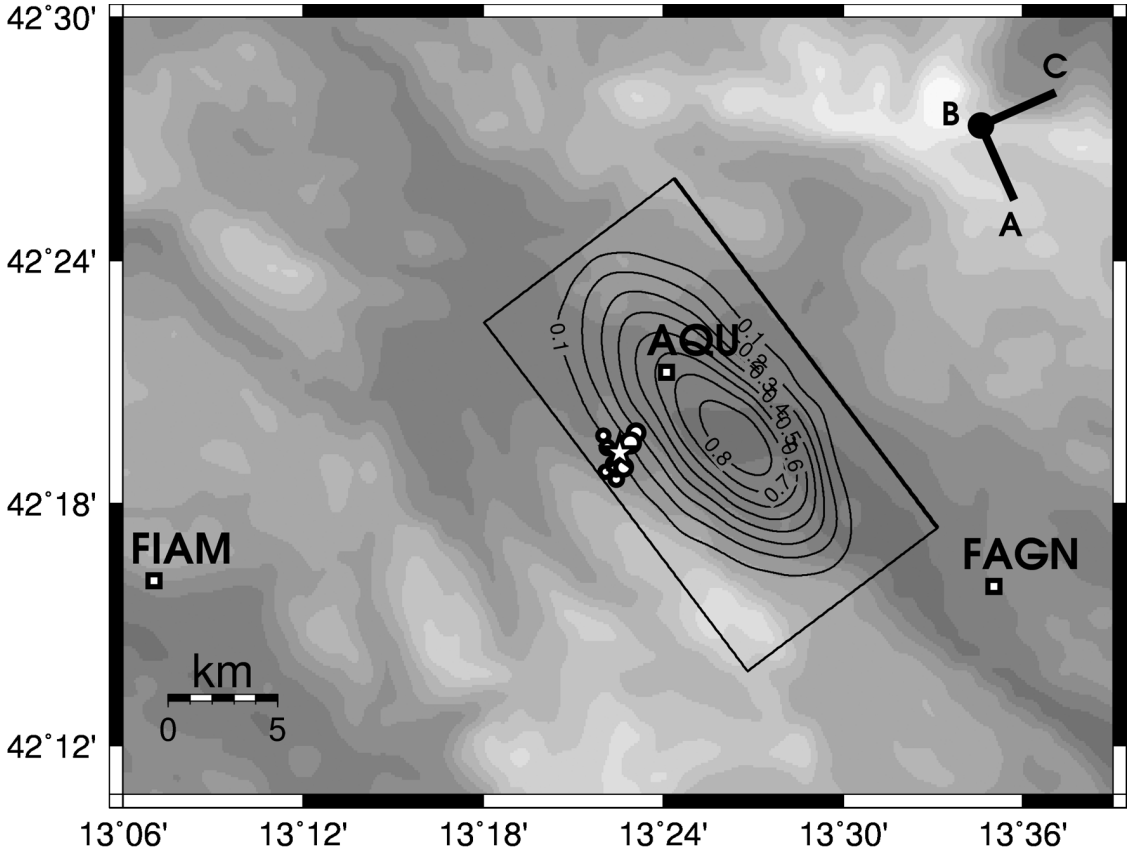

Fig. 1 - Map of the epicentral region of the April 6, 2009 L'Aquila earthquake with the fault geometry and slip distribution from the work by Walters *et al*. (2009). Large solid circle (B), location of the two interferometers; solid lines (BA and BC), directions of the interferometers. Star, epicenter of the March 30 M 4.1 foreshock; circles, epicenters of the succeeding foreshocks with $M > 2.5$ [http://iside.rm.ingv.it]. DEM data from http://srtm.csi.cgiar.org.

instrument length, and Δl is positive for an increase in length. We use the symbol nε, nanostrain, for $\Delta l/l = 10^{-9}$. The instruments are characterized by very high sensitivity (better than picostrain level), a wide frequency band (from d.c. up to hundreds of Hz), and a large dynamic range, limited only by the capability of maintaining the optical alignment. Each interferometer is based on the classical unequal-arm Michelson set-up and compares the optical length (i. e., the length expressed in terms of the light wavelength) of a longer measurement arm (90 m in length) and a shorter fixed reference arm that is 20 cm long. Extension is measured with respect to the baseline length at the starting time of each record. Thus an arbitrary strain value can be added to any strain time series.

Till February 2005, the reference arm included an electro-optical phase modulator, consisting of an optically active crystal whose optical length depends on the electric field embedded in. The electric field was dynamically modulated by a feedback loop to stabilize the interference pattern between the laser beams propagating through the reference and measurement arms. The intrinsically small dynamics of the phase modulator had been overcome by changing its optical

thickness by one wavelength each time the phase shift is + π or - π. The jumps prevented the interferometers from working for about 50 μs. When no jump was involved, the bandwidth reached a few hundred kHz (Crescentini and Renzella, 1991). Voltage applied to the phase modulator was sampled at 800 Hz by a 12-bit digital-to-analog converter. Each datum consisted of two numbers, the former related to the voltage applied to the phase modulator, and the latter related to the number of jumps from the start of the acquisition. Both sequences of numbers were digitally filtered using a linear non-recursive filter, decimated at 5 Hz, and recorded. Such a configuration allowed recording data at any frequency, after applying a proper low-pass digital filter to the two above-mentioned sequences of numbers. This feature of the apparatus was particularly useful in the past, when local storage of a huge amount of data was a difficult task, but it requires expensive electro-optical components, a very accurate optical alignment and electronic adjustment, and an occasional careful data pre-analysis to correct for wrong jump counting. From February 2005 to May 2006 the experimental set-up underwent major changes, and present electro-optical configuration is much simpler: the reference arm includes only what is required to get two quadrature signals at one output for each interferometer [the other output is not used, differently from Crescentini and Amoruso (1996)] i. e., a polarizer and a quarter-wave retarder plate. Also the electronics are now much simpler, consisting only in what is necessary to measure light intensity at the photodiodes. As a drawback, phase mismatch (which is proportional to strain) is no longer linearly related to the ADC output, which in turn can not be simply low-passed and decimated before storage. Real time conversion from light intensity to phase (i. e., strain) is not possible, because instabilities of the DC level and amplitude of the interference signal as well as phase lag fluctuations between the quadrature signals ask for a non-linear fit of the Lissajous figure given by a few hours of data. Photodiode outputs are sampled and stored at 600 Hz to avoid artificial mixing of frequencies due to the non-linear dependence of light intensity on phase mismatch, and intensity-to-phase conversion is accomplished on stored signals when needed. Changes did not degrade instrumental performances.

Although the interferometer measures strain directly, local distortions, such as cavity effects due to tunnel installation, surface topography, and inhomogeneities in elastic constants, can bias strain measurement significantly, even if they do not add stochastic noise. Moreover, deformations due to the seasonal dynamics of the local aquifer adds to “genuine” strain signals. Cavity effects are expected to be small on both interferometers, since they measure extension along the axis of two tunnels and the distance between the end-monuments and the tunnel end faces are more than one tunnel diameter. Topographic effects are expected to be small on BA, but as large as 20% to 40% on BC, since BA is approximately parallel to the local trend of the Apennines mountain chain and BC is approximately perpendicular to it. Siting effects can also produce coupling among the different strain components, so that measured strain is not equal to the large-scale Earth strain. Strain distortions can be estimated under the assumption that the scale of these effects is much smaller than the scale of the measured stress and strain perturbations (e.g., Park *et al*., 2008). Estimates of local effects using reference Earth tide strains show faint coupling among the different strain components, but, as expected, strain measured along BC is reduced by about 30% because of topographic effects. Air pressure and temperature along the tunnel are also recorded; their (small) effects and, when appropriate, deformation associated to tides, are removed from strain data (Agnew, 1997; Amoruso *et al*., 2000; Tamura

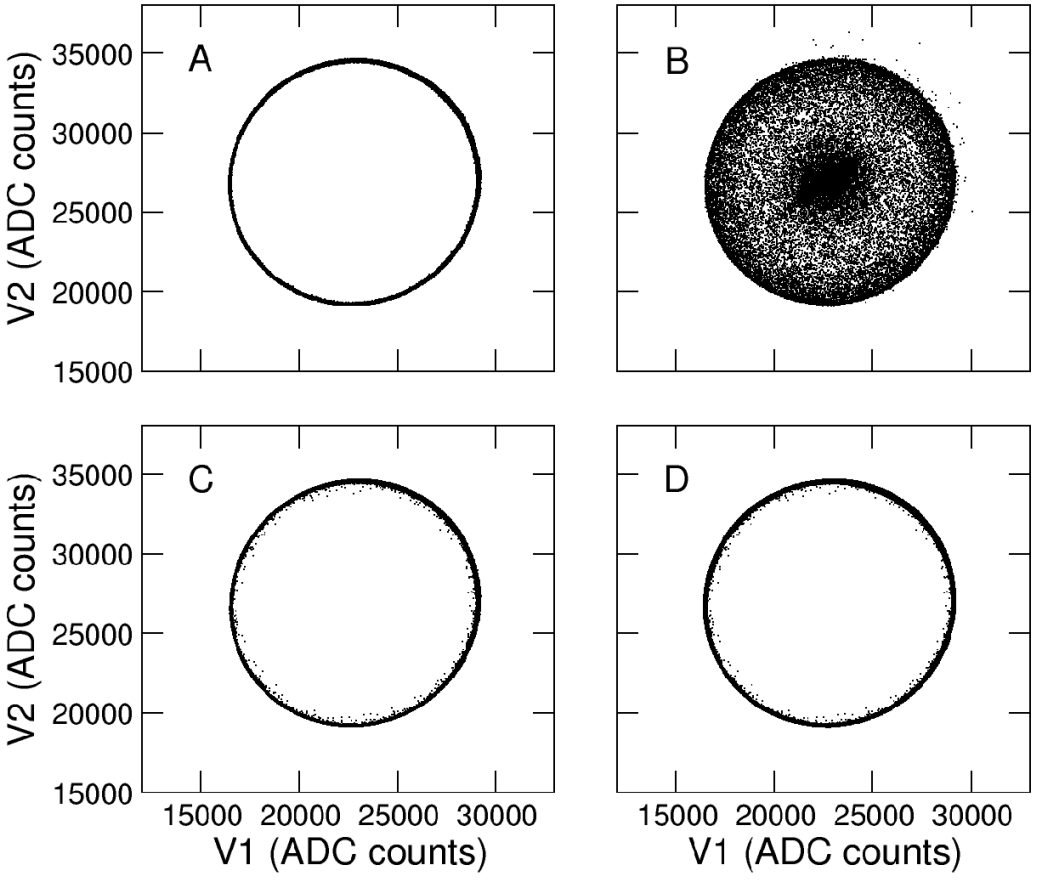

Fig. 2 - Lissajous figures given by the two outputs of interferometer BA (600 samples per second): A) during 2000 s immediately before the earthquake; B) 58 s throughout major shaking; C) 880 s immediately after it, and D) for the periods A and C.

and Agnew, 2008). Last but not least, in an unequal-arm Michelson interferometer whose measurement arm is much longer than the reference arm, strain in the measurement arm and fractional changes in wavelength (or frequency) of the laser light are numerically equivalent. This means that a change in the laser light wavenumber cannot be distinguished from a change in the length of the measurement arm. Laser frequency fluctuations can give spurious strain signals whose amplitude depends on the difference in length between the measurement and reference arms. Since the two interferometers share the same laser source, these spurious wavelength fluctuations are coherent in the two interferometers and disappear in the difference between the two measured strains. This noise cancellation behavior implies that signal-to-noise should be higher for measured deviatoric strain than for horizontal expansion or contraction.

Before, during and after the April 6, 2009 L'Aquila earthquake, the two interferometers (baseline BA approximately parallel to the strike of the 2009 L'Aquila earthquake, and baseline BC approximately perpendicular to it, Fig. 1) continuously maintained the optical alignment [see Fig. 2 and Amoruso and Crescentini (2010)]. Unfortunately, because of low-pass filters in the

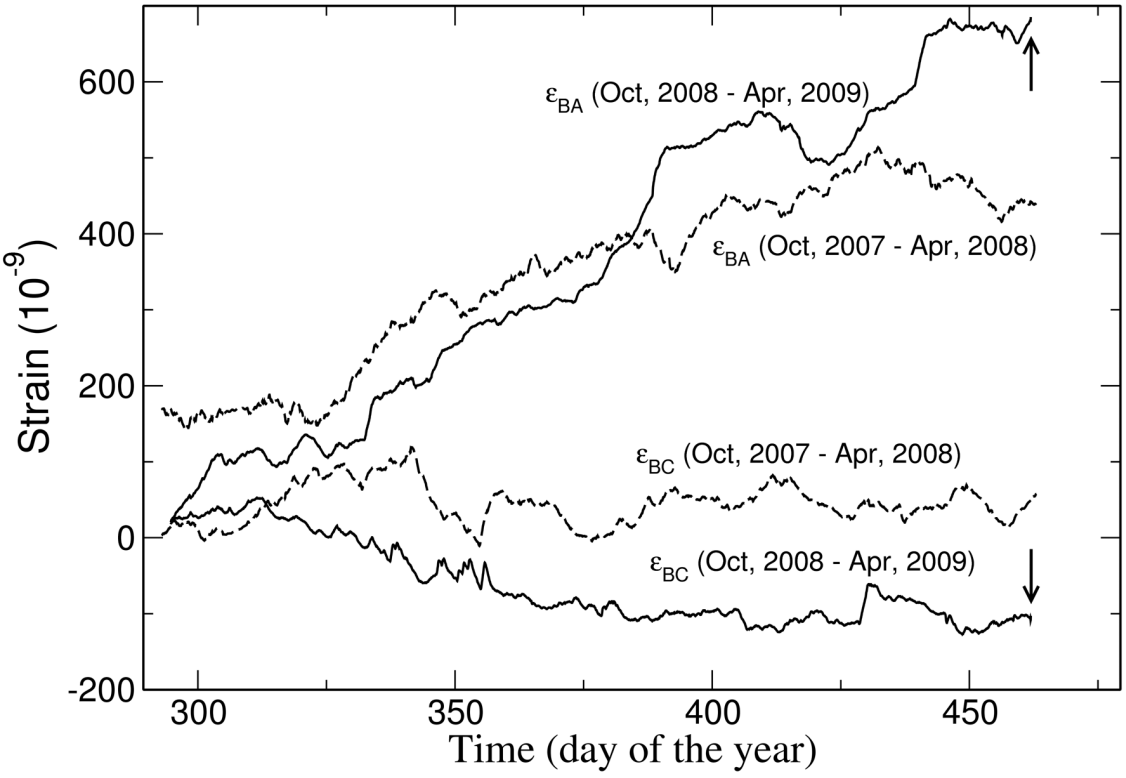

Fig. 3 - Comparison of strain recorded at both interferometers during the periods October 2008 to April 6, 2009, and October 2007 to April 2008. Zero-strain level for each time series is arbitrary. No coherent anomalous signal larger than a few tens of nanostrains is visible during the months preceding the earthquake. Arrows, occurrence time of the earthquake.

electronic set-up, the Lissajous figure collapses into a small confused one during fast oscillations of the interference fringes (see Fig. 2, panel B), so that the interferometers are effectively blind when the strain rate is faster than a few hundred nanostrains per second. An analogous limitation is also given by the sampling rate (600 samples per second) because if the phase change rate is faster than about 10^5 deg/s, then the phase lag between two consecutive data is larger than 180°, giving rise to an intrinsic ambiguity in strain reconstruction. This limitation did not allow the reliable recording of co-seismic offsets due to the main shock and major aftershocks, vibrations during major shaking of the main shock (about 80 s in duration), and the co-seismic offset due to the March 30th *M* 4.1 foreshock (about 30 ambiguous data).

The possible existence of different pre-seismic, strain-producing phenomena has to be searched for in different time-scales. Since the noise of strain measurements increases with period (e.g., Agnew, 1992; Crescentini *et al*., 1997), the strictness of the constraints depends on the time interval considered (and, of course, on the distance of the strain meter from the source).

In looking for possible precursory activity on the scale of months, the strain recorded from October 2008 to April 6, 2009 has been analysed and compared to the analogous period of the previous year (October 2007 to April 2008) due to the presence of seasonal effects. Fig. 3 shows

data after removal of Earth tides and environmental effects, and shifting the zero-strain level for each time series arbitrarily; no indication of coherent anomalous signals larger than a few tens of nanostrains is envisaged. To put constraints on the volume of the possible earthquake preparation zone, i. e., an inclusion suffering changes in the elastic properties of the crustal rock, the small perturbation method has been used to find an approximate solution of the superficial displacement caused by an inclusion for an otherwise homogeneous isotropic elastic half-space. We start from Dobrovolsky *et al*. (1979) and, for an extensional tectonic regime, we obtain:

$$w_r(x_0, y_0) = -\left[\frac{\Delta K}{K^\circ}\frac{\sigma^\circ_u}{3}\delta_i^j + \frac{\Delta\mu}{\mu^\circ}\left(\sigma^\circ_{ij} - \frac{\sigma^\circ_u}{3}\delta_i^j\right)\right]\iiint v\ v^r_{i,j}dV \qquad (1)$$

where $\overrightarrow{w}$ is the displacement vector at the point (x_0, y_0), K° is the bulk modulus outside the inclusion, μ° is the shear modulus outside the inclusion, $\Delta K + K^\circ$ is the bulk modulus inside the inclusion, $\Delta\mu + \mu^\circ$ is the shear modulus inside the inclusion, v^r_i is the displacement tensor at (x,y,z) of a unit point force acting on (x_0, y_0) and computed in an elastic half-space (e.g., Mindlin, 1936) (direction and versus of the point force are the same as the displacement vector); σ°_{ij} is the tectonic stress field, uniform at large distances. Suffixes preceded by a comma denote differentiation and repeating tensor indexes imply summation. Volume integral is discretized and strain tensor elements are computed through proper differentiation and combination of the displacement vectors for point volumes, located in different positions of the plane of the causative fault of the April 6, 2009 earthquake. Hereinafter, we use μ°=30 GPa and consider the rock outside the inclusion as a Poisson solid.

Estimate of high- and low-frequency effective elastic moduli of dry or saturate porous or cracked rocks can be performed following Le Ravalec *et al*. (1996), for specific pore/crack geometries (idealized spheres and ellipsoids). Crack density (ϕ) and water saturation affect both the bulk and shear moduli, even if at different levels. Cracks are more compressible than round pores, and, when fluid pressure gradients are induced, pore fluid flows from the most pressurized regions (cracks) to the least ones (round pores). At low frequencies there is enough time for fluids to flow between pores and cracks, so that fluid pressure equilibrates. On the contrary, at high frequencies, fluid can no longer flow, and fluid pressures are unequilibrated; the "boundary" frequency (f_c) is approximately $f_c \approx \alpha^3 K_S/\eta_f$, where α is the crack aspect ratio, η_f is the fluid viscosity, and K_S is the solid bulk modulus, corresponding to an initial matrix where there are no pores. Although f_c is strongly dependent on the crack aspect ratio (α), in our case the low-frequency assumption is always satisfied.

For estimating the maximum volume of possible inclusions in the source area, we have to assess the sensitivity of our data, i. e., our detection threshold. We have computed strain changes at the interferometer site generated by small inclusions on a regular grid around the hypocenter, for an extensional tectonic stress σ=10^8 Pa acting perpendicularly to the fault strike, and V=1 km^3. The shear modulus depends on the crack density only, while the presence of a very small amount of air (or gas) within the pore space is sufficient to induce a drastic decrease of the bulk modulus (Le Ravalec *et al*., 1996). We use ϕ=0.1 (~7% decrease of shear wave velocity) and consequently $\Delta\mu/\mu^\circ \approx$-0.13, $\Delta K/K^\circ \approx$-0.05 for saturated rock, $\Delta K/K^\circ \approx$-0.26 for unsaturated rock

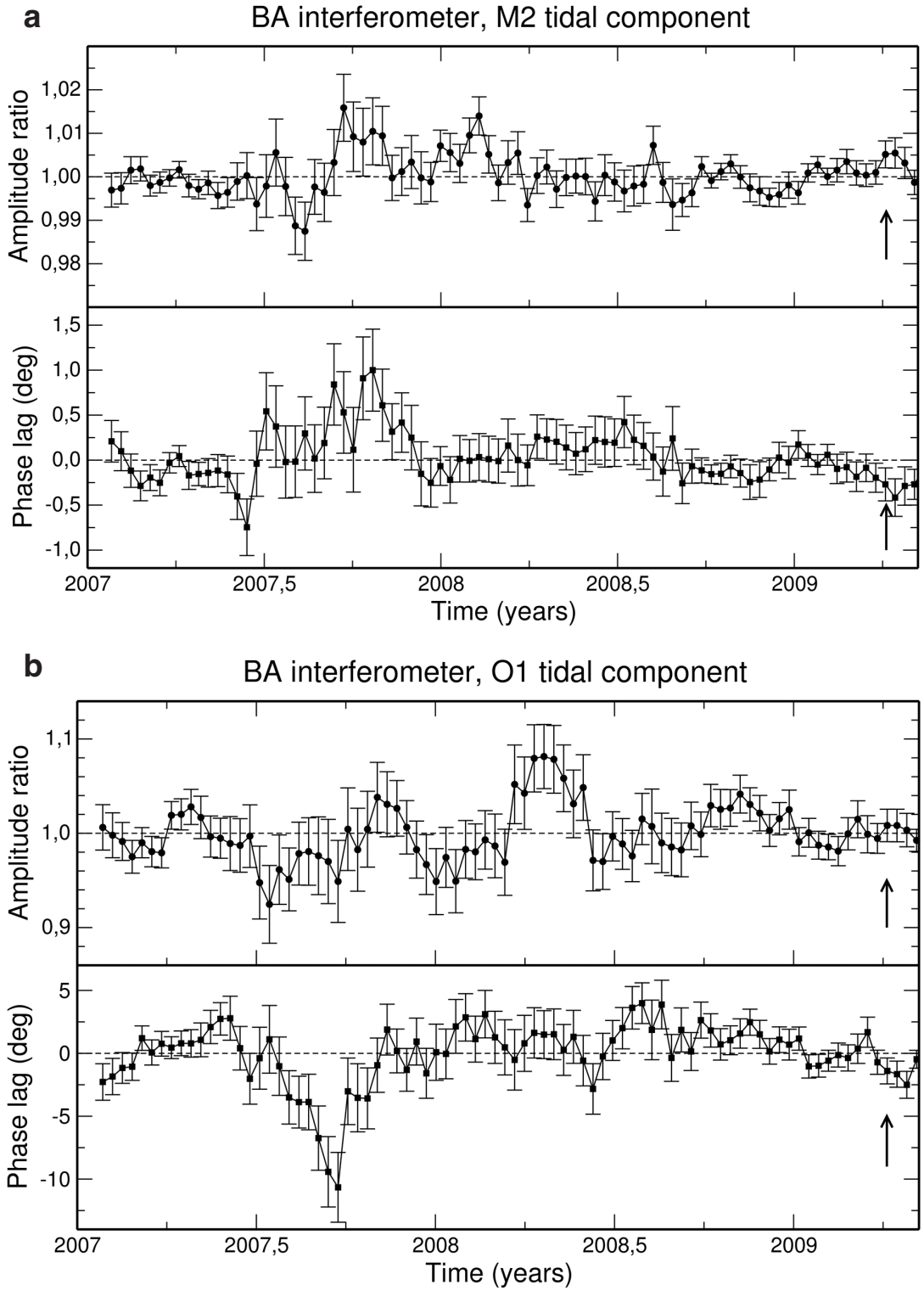

Fig. 4 - Tidal response as a function of time, BA interferometer. Upper panel, M2 component; lower panel, O1 component. Sliding 2-month time blocks were used with a 10-day overlap between blocks. Error bars are 1 standard deviation. Amplitude normalized to the weighted mean value; phase lag given with respect to the weighted mean value. Arrows, occurrence time of the earthquake.

(Le Ravalec *et al*., 1996). Computed strain changes are at the nε level for both interferometers. Comparison of the strain recorded during the periods October 2008 to April 6, 2009, and October 2007 to April 2008 shows no indication of coherent anomalous signals larger than a few tens of nanostrains (Fig. 3) thus limiting the volume of the possible inclusion to less than 100 km^3.

Although we can not completely exclude that a large-scale pre-seismic phenomenon took place, it seems unlikely. Further support to this conclusion is given by the lack of detectable changes in Earth tidal response before the earthquake. Signal-to-noise ratio of the Gran Sasso interferometers in the tidal band is very high, and we determine the tidal response for the two years prior to the L'Aquila earthquake. The tidal analyses have been carried out using VAV2003 (Venedikov *et al*., 2005) on sliding 2-month time blocks with a 10-day overlap between the blocks. The time tag associated with each analysis is taken as the midpoint of the window. Fig. 4, upper panel, shows the amplitude and phase of M2 for BA interferometer (see Fig. 5, upper panel, for the BC interferometer) as a function of time from 2007 to summer 2009. Higher noise from June 2007 to February 2008 reflects anthropic activity close to the interferometers. The best signal-to-noise ratio is achieved in the case of the BA interferometer, and no change in the tidal response is visible before the earthquake, within 0.5% in amplitude and 0.5° in phase. The analyses of the M2 tidal response for BC lead to the same conclusion, even if with a lower signal-to-noise ratio, as well as the O1 tidal response for both interferometers (Figs. 4 and 5, lower panels).

Excluding the existence of a large-scale pre-seismic phenomenon does not necessarily contradict some recently-published anomalies preceding the April 6, 2009 L'Aquila earthquake. Predictory radon anomalies that have been claimed (Giuliani *et al*., 2009) are far from being well grounded, even if Giuliani's interviews attracted the attention of the international scientific community. The existence of radon peaks is not surprising during a period of seismic activity, but, as promptly stressed by Kerr (2009), in a prediction scheme, an earthquake follows a notable radon peak. In the scant documentation (radon records are too short) produced by Giuliani, there are too many peaks and those associated with supposedly precursory radon are no different (at least not obviously different) from the others. Moreover, no correlation between the size of the peaks and the magnitudes of the subsequent earthquakes can be envisaged. Reported radio anomalies (Biagi *et al*., 2009) might be due to an interruption of the broadcasting from the transmitter (RMC, France) (P. Tognolatti, personal communication; Biagi *et al*., 2010). As regards the reported uranium (U) anomalies in the groundwater collected weekly from June 2008, inside the LNGS (Plastino *et al*., 2010), the presence of U in the groundwater at Gran Sasso is directly linked to the presence of the so-called terra rossa inside the karstified fissures in the rock above the laboratory. Terra rossa is thought to be the weathering product of limestone dissolution and/or formed by accumulation of detrital mud, ash, or dust on preexisting karst limestones, and/or (as more recently suggested) formed by replacement of limestone by authigenic clay (Merino and Banerjee, 2008). The karstified fissures in the rock above the laboratory represent preferential groundwater flowpaths [Laubenstein and Magaldi (2008), Adinolfi *et al*. (2008), see also the schematic section of the Gran Sasso carbonate aquifer close to the underground laboratories in Adinolfi *et al*. (2008)]. U groundwater concentration depends on the type and degree of fracturing and karstification, and on the water-rock interaction time. The U time series (Plastino *et al*., 2010) are actually very similar at all sites (E1, E3, E3dx, and E4), the only exception being

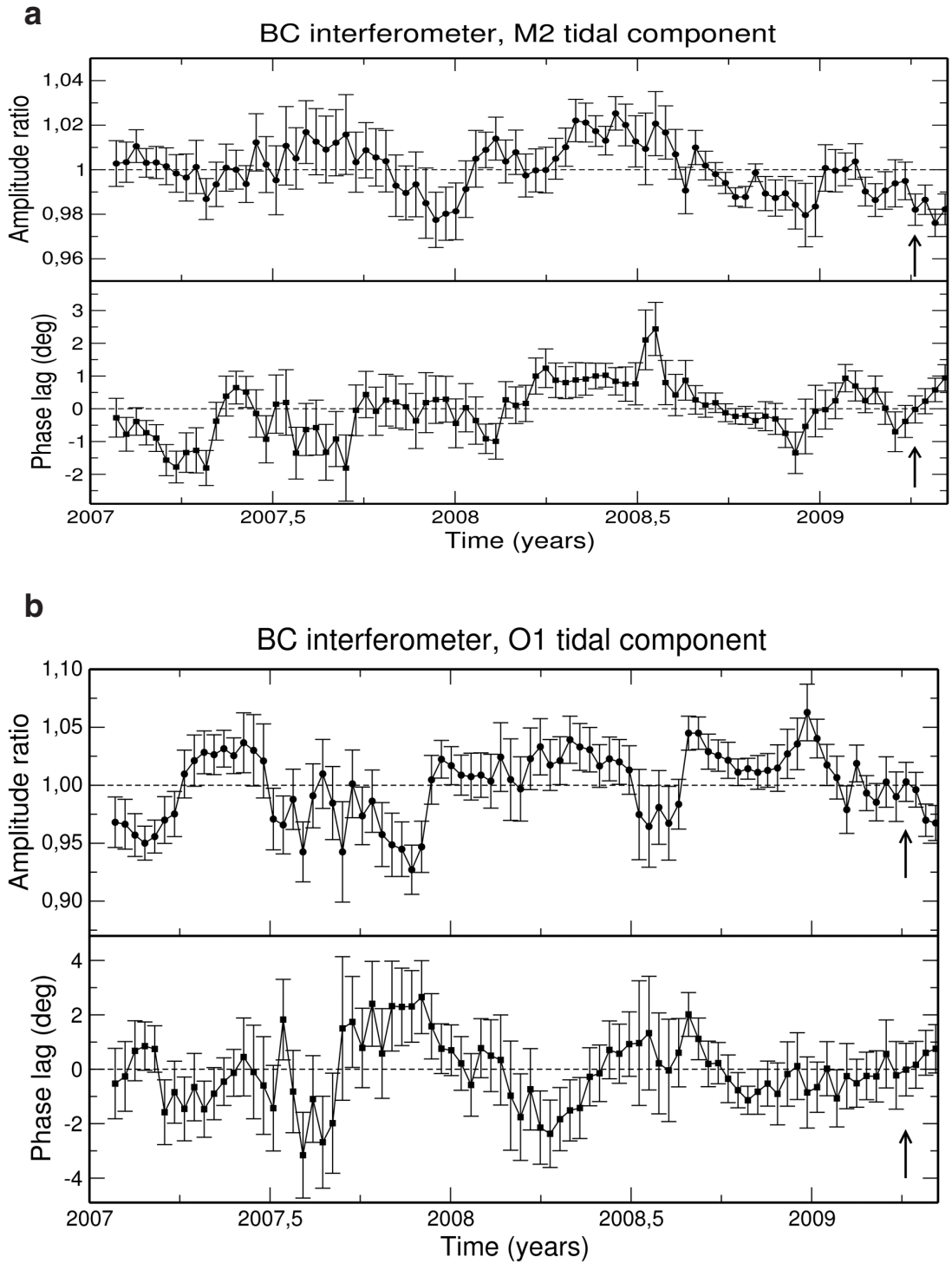

Fig. 5 - Tidal response as a function of time, BC interferometer. Upper panel, M2 component; lower panel, O1 component. Sliding 2-month time blocks were used with a 10-day overlap between blocks. Error bars are 1 standard deviation. Amplitude normalized to the weighted mean value; phase lag given with respect to the weighted mean value. Arrows, occurrence time of the earthquake.

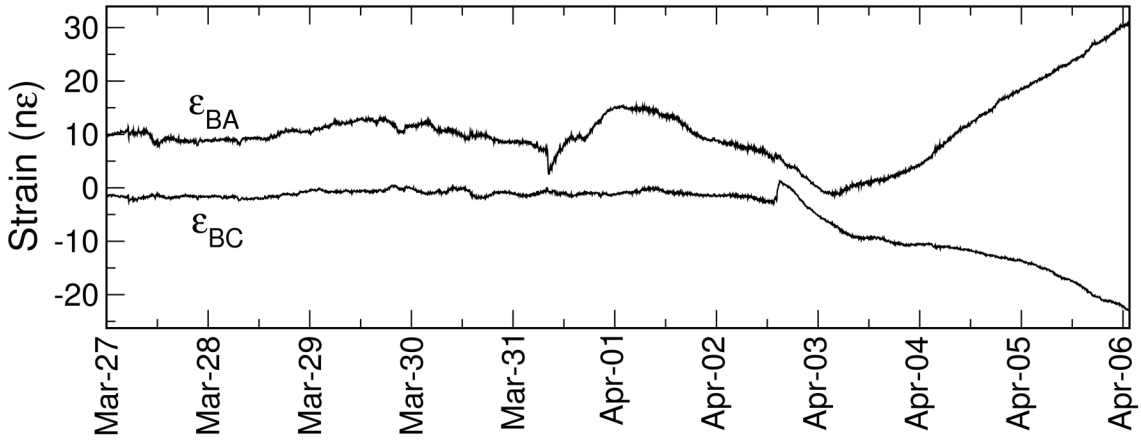

Fig. 6 - Last ten days before the earthquake. Data have been low-pass filtered with a 10-pole Butterworth filter with a high cut of 1.67 10^{-3} Hz and the linear trend of the first 6 days removed. The apparent anomalies in BA and BC, that occurred about 5.7 and 3.5 days before the earthquake, are due to anthropic activity related to nearby experiments close to A and C end monuments respectively. The figure ends at the first P arrival.

two spikes at E3dx during summer 2008. Moreover each U time series, if properly scaled, strictly mimics those of Na, Ca, and Mg at the same site [Plastino *et al*. (2009); see also Figs. S01 and S02 in the Auxiliary Material of Amoruso and Crescentini (2010)], suggesting, at a first glance, possible, mere changes in water recharge and dilution and/or dissolution (e.g., because of CO_2 increase). However, a CO_2 increase seems unsupported by the pH time series, and the ionic-content time series appear inconsistent with the electrical conductivity ones [see plots in Plastino *et al*. (2009, 2010)].

For a closer look at a day-period, possible precursory activity, Fig. 6 shows the strain recorded during the last 10 days before the earthquake, after removal of Earth tides, environmental effects, and co-seismic offsets (due to foreshocks). Data have been low-pass filtered with a 10-pole Butterworth filter with a high cut of 1.67 mHz and the linear trend of the first 6 days has been removed. It should be noticed that the apparent anomalies in BA and BC, occurred about 5.7 and 3.5 days before the earthquake, and are due to anthropic activity close to A and C end monuments (related to nearby experiments), respectively,. There are some hints of coherent (but opposite in sign) changes in the last 3 to 4 days preceding the earthquake, but it is difficult to provide a quantitative evaluation of how likely such variations relate to the earthquake. They are similar to coherent strain-rate changes that occurred at least twice during the last 6 months before the earthquake, and could be casual or ascribable to other causes such as the local aquifer. Nevertheless, these changes are significant in this section of the record and the possibility that they may result from some pre-seismic or post-seismic (with respect to the *M* 4.1 foreshock that occurred on March 30 close to the April 6 mainshock, Fig. 1) process cannot be precluded. As already mentioned, Di Luccio *et al*. (2010) report a ~5% increase of V_p/V_s along the path between the seismic stations AQU and FAGN (Fig. 1), which is parallel to the NW-SE striking earthquake causative fault, during the days preceding the main shock, while changes along the NE-SW

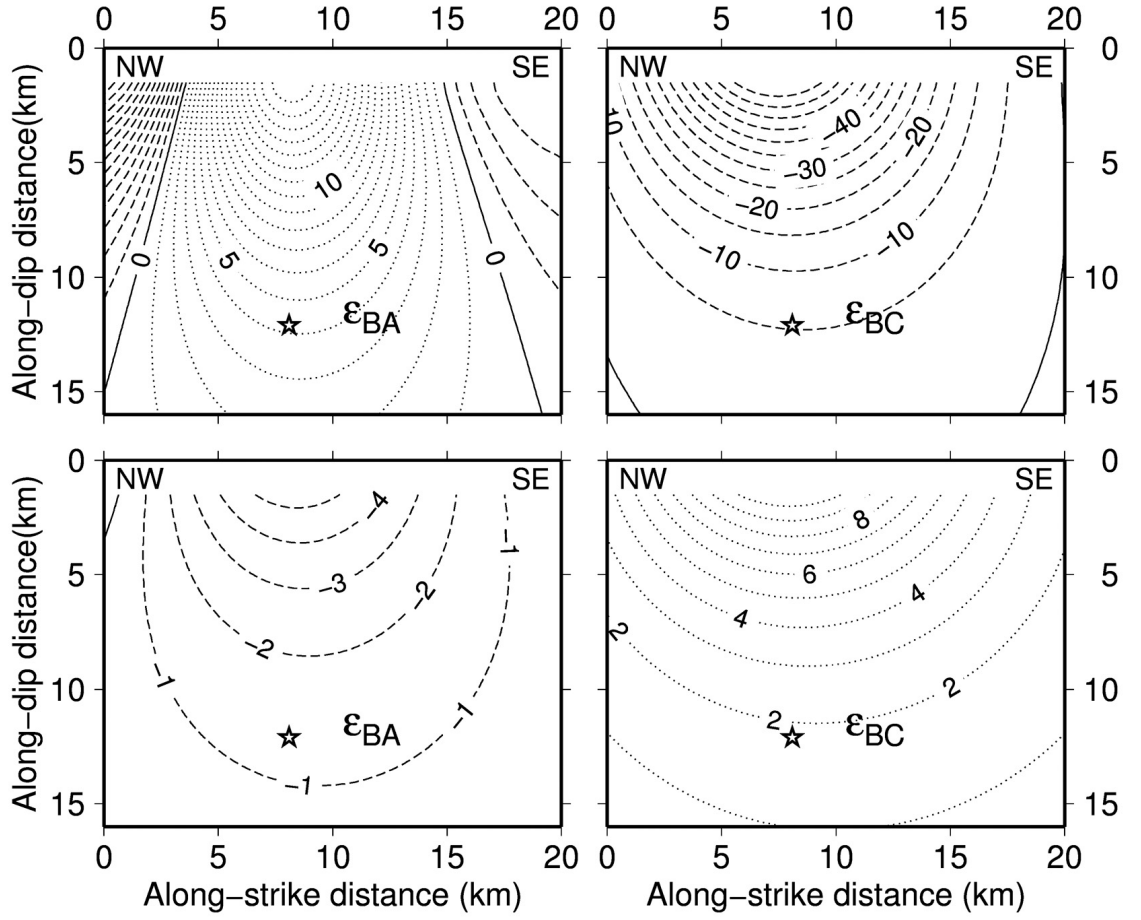

Fig. 7 - Strain (nanostrains; dashed contours, negative values; dotted contours, positive values) generated at the interferometers by a small inclusion (V = 1 km^3) located in different positions on the fault plane in Fig. 1. Star, hypocenter of the March 30 foreshock. Top panels: case A (dilatancy of saturated rock, see text for details). Bottom panels: case B (saturation of unsaturated cracked rock, see text for details).

striking path between AQU and FIAM were certainly much smaller or null. Such observations have been ascribed to the movement of fluids along fault planes. To test the consistency of our data with this observation, we computed possible strain (due to the increase of V_p/V_s) on BA and BC, modeled through fluid migration and crack opening in saturated rocks (case A) or saturation of partially saturated rock (case B). Following Fig. 5 in Le Ravalec *et al*. (1996), for a ~5% increase of V_p/V_s, in case A the shear modulus (μ) would decrease by about 22% and the bulk modulus (K) by about 8%, while in case B, μ would remain unchanged and K would increase by about 20%. We modelled such phenomena through computation of the amplitude and sign of deformation at both interferometers due to small inclusions (V=10^9 m^3) located in different positions on the fault plane in Fig. 1 (Walters *et al*., 2009), for both cases A and B (Fig. 7), using a simple homogeneous half-space approximation. Moreover, because of the model simplicity, we do not take into account local effects. As can be seen from Fig. 7 (top panels), saturated-rock

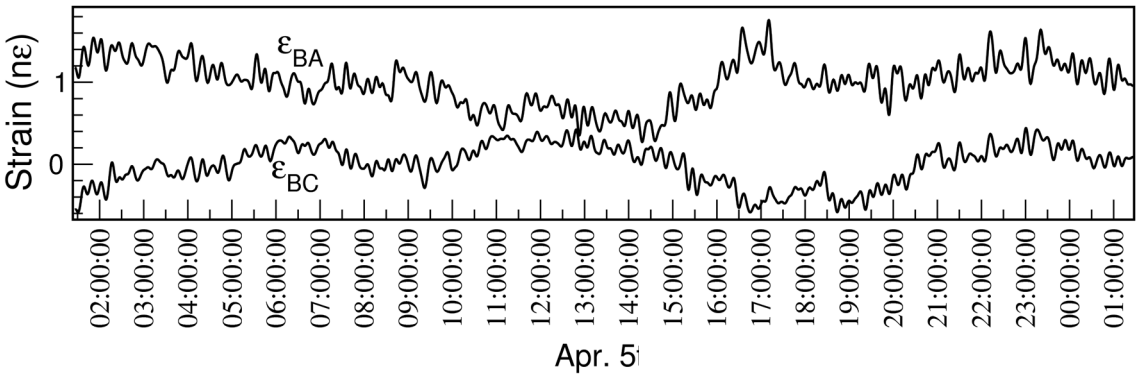

Fig. 8 - Last day before the earthquake. Data have been low-pass filtered with a 10-pole Butterworth filter with a high cut of $1.67 \cdot 10^{-3}$ Hz and detrended. The figure ends at the first P arrival.

crack opening in the region surrounding the March 30 foreshock causes negative BC strain and positive BA strain, of about the same amount (nanostrains). Comparing this result with observed strain changes (~10 nε in amplitude) observed during the days preceding the earthquake (Fig. 7), a dilatant volume of about 10 km^3 would be involved. Such a source is quite small and unable to justify the observations in Di Luccio *et al*. (2010) if quasi-spherical in shape, but consistent with them in the case of movement of fluids along the fault plane, i. e., if it is confined to a thin sheet over the fault plane. Possible explanations include the occurrence of a sudden dilation, and the corresponding changes in porosity, permeability and fluid pressure, and thus fluid flows - caused by the *M* 4.1 foreshock (March 30) and/or the succeeding foreshocks (Fig. 1) - into and along the fault. On the contrary, as can be seen from Fig. 7 (bottom panels), saturation of partially saturated rock both in the region surrounding the March 30 foreshock and elsewhere on the fault plane causes negative BA strain and positive BC strain, in full disagreement with our observations.

The analyses of the data closer in time to the earthquake occurrence can put limits to the nucleation phase. As predicted by theoretical models, to be linked to nucleation at the earthquake hypocenter, precursory strain could be detectable as rapid acceleration of strain near instability, either because of local dilatancy (days before the earthquake, e.g., Rice and Rudnicki, 1979) or nucleation zone expansion (from tens to hundreds of seconds before the earthquake, e.g., Fang *et al*., 2010), the strain history should be exponential-like with the largest strain changes occurring at the last stages of failure and the amplitude or size of the strain change relating to nucleation patch moment release. Moreover, changes have to be present in both (BA and BC) strain time series. From Fig. 3 in Amoruso and Crescentini (2009b), strain arising from slip on a plane containing the source fault can be estimated. In particular, Fig. 3 in Amoruso and Crescentini (2009b) shows the expected amplitude and sign of deformation at both interferometers due to very small sub-faults (M_o = $2.5 \cdot 10^{16}$ Nm) located in different positions on the fault plane in Walters *et al*. (2009), using a simple homogeneous half-space approximation (Poisson ratio 0.29; rigidity $2 \cdot 10^{10}$ N/m^2) and taking into account siting effects. If nucleation occurs at the earthquake hypocenter, a $2 \cdot 10^{15}$ Nm normal-faulting source produces $\varepsilon_{BA} \approx 1$ nε and $\varepsilon_{BC} \approx$ -1 nε, to be compared with Fig. 8, where the last day of data, lowpass filtered with a 10-pole Butterworth filter with a high cut of $1.67 \cdot 10^{-3}$ Hz and detrended, is shown. Since no coherent exponential-like

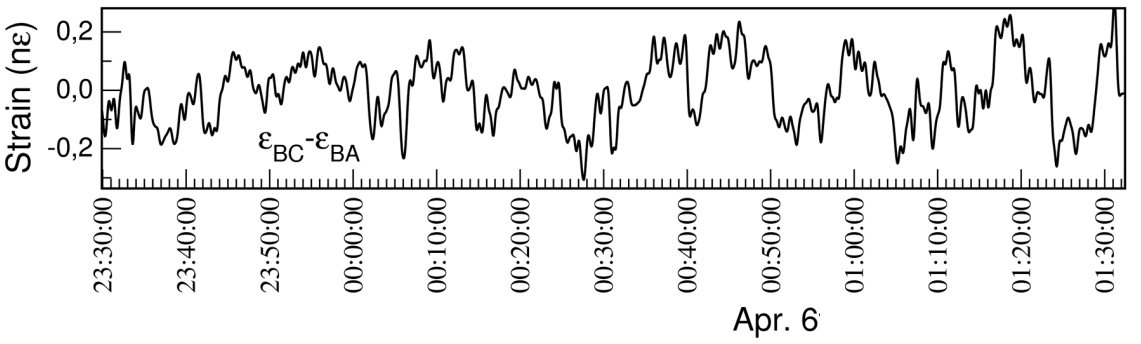

Fig. 9 - Last two hours before the earthquake. Data have been low-pass filtered with a high cut of 0.033 Hz and detrended. The figure ends at the first P arrival.

changes larger than 1 nε are apparent, the largest moment release that could go undetected is $2 \cdot 10^{15}$ Nm.

Closer and closer to the earthquake occurrence time, i. e., hours preceding the first P wave arrival, laser frequency fluctuations become a major error source. Since the two interferometers share the same laser source, these spurious effects are coherent in the two interferometers and disappear in the difference between the two measured strains. Consequently, Fig. 9 shows ε_{BC} - ε_{BA} in the two hours preceding the first P arrival. Data have been lowpass filtered with a high cut of 0.033 Hz and detrended, and it is evident that possible nucleation strain changes are smaller than standard deviation (0.1 nε, in this case). Thus the largest moment release that could go undetected is $2 \cdot 10^{14}$ Nm. Fig. 10 shows ε_{BC} - ε_{BA} during ten seconds preceding the first P arrival. Data have been lowpass filtered with a 10-pole Butterworth filter with a high cut of 10 Hz; 6 harmonics in the microseism band [surface waves generated at sea, Agnew (1986)] have been removed, at periods of 1.3, 2.0, 2.2, 3.7, 4.5, and 5.0 secs, using the Least Squares Spectral Analysis [LSSA code: Pagiatakis (1999)]. Again, possible nucleation-related strain changes are smaller than standard deviation (10^{-3} nε, in this case), thus strain changes immediately before the earthquake are less than 1 picostrain, and the largest moment release that could go undetected is $2 \cdot 10^{12}$ Nm. In summary, the largest moment release that could go undetected is $2 \cdot 10^{15}$ Nm during one day before the event, $2 \cdot 10^{14}$ Nm during two hours, $2 \cdot 10^{12}$ Nm during ten seconds before the event, to be compared with the earthquake seismic moment that is about $3.5 \cdot 10^{18}$ Nm (Cirella *et al*., 2009). Seconds before the event, the seismic moment release that could go undetected was less than 0.00005% of the earthquake seismic moment. Estimate of the size of the nucleation zone can be done, e.g., under the assumption of constant stress drop [recently reinforced by Shaw (2009)], and for a nucleation moment release lower than about $2 \cdot 10^{12}$ Nm, we get a source size of the order of tens of meters, i. e., much much smaller than that of the earthquake, in agreement with the results obtained by Johnston *et al*. (2006) for the 2004 Parkfield earthquake. Thus, also the 2009 L'Aquila earthquake has been triggered by failure of small localized zones, and the earthquake fault model must be inhomogeneous.

Our work places new constraints on the earthquake source behavior and phenomena proposed by others to be precursive to the April 6, 2009 L'Aquila earthquake. In particular, we establish

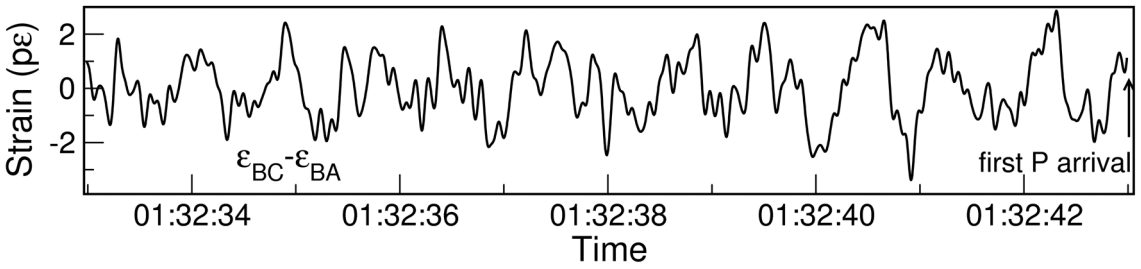

Fig. 10 - Last ten seconds preceding the first P arrival. Data have been low-pass filtered with a 10-pole Butterworth filter with a high cut of 10 Hz; 6 harmonics in the microseism band have been removed, at periods of 1.3, 2.0, 2.2, 3.7, 4.5, and 5.0 s. The figure ends at the first P arrival.

limits on any possible precursory deformation. While there have already been previous efforts focused here (e.g., Johnston *et al*., 2006), we present a rather more sophisticated approach to the physics of the modeling and we lower the thresholds for any such precursory activity significantly. Our work does not imply that precursory phenomena do (or did) not exist at all: predicting earthquakes is challenging and maybe possible in the future, but all the researches have to be performed following strictly objective scientific criteria.

Acknowledgments. The paper was presented at the 28th Convegno Nazionale GNGTS. The Gran Sasso strainmeters were supported by the Accordo di Programma INGV-INFN.

REFERENCES

Abercrombie R.E., Agnew D.C. and Wyatt F.K.; 1995: *Testing a model of earthquake nucleation.* Bull. Seismol. Soc. Am., **85**, 1873-1878.

Adinolfi Falcone R., Falgiani A., Parisse B., Petitta M., Spizzico M. and Tallini M.; 2008: *Chemical and isotopic ($\delta^{18}O‰$, $\delta^{2}H‰$, $\delta^{13}C‰$, ^{222}Rn) multi-tracing for groundwater conceptual model of carbonate aquifer (Gran Sasso INFN underground laboratory - central Italy).* J. Hydrol., **357**, 368-388.

Agnew D.C.; 1986: *Strainmeters and tiltmeters*. Rev. Geophys., **24**, 579-624.

Agnew D.C.; 1992: *The time-domain behavior of power-law noises.* Geophys. Res. Lett., **19**, 333-336.

Agnew D.C.; 1997: *NLOADF: a program for computing ocean-tide loading*. J. Geophys. Res., **102**, 5109-5110.

Amoruso A. and Crescentini L.; 2009a: *The geodetic laser interferometers at Gran Sasso, Italy: recent modifications and correction for local effects.* J. Geodyn., **48**, 120-125, doi: 10.1016/j.jog.2009.09.025

Amoruso A. and Crescentini L.; 2009b: *Slow diffusive fault slip propagation following the 6 April 2009 L'Aquila earthquake, Italy.* Geophys. Res. Lett., **36**, L24306, doi: 10.1029/2009GL041503.

Amoruso A. and Crescentini L.; 2010: *Limits on earthquake nucleation and other preseismic phenomena from continuous strain in the near field of the 2009 L'Aquila earthquake.* Geophys. Res. Lett., **37**, L10307, doi: 10.1029/2010GL043308.

Amoruso A., Crescentini L. and Scarpa R.; 2000: *Removing tidal and atmospheric effects from Earth deformation measurements*. Geophys. J. Int., **140**, 493-499.

Ampuero J.-P. and Rubin A.M.; 2008: *Earthquake nucleation on rate and state faults - Aging and slip laws.* J. Geophys. Res., **113**, B01302, doi: 10.1029/2007JB005082.

Bernard P., Boudin F., Sacks S., Linde A., Blum P.-A., Courteille C., Esnoult M.-F, Castarede H., Felekis S. and Billiris H.; 2004: *Continuous strain and tilt monitoring on the Trizonia Island, Rift of Corinth, Greece.* Compt. Rend. Geosci., **336**, 313-323.

Beroza G.C. and Ellsworth W.L.; 1996: *Properties of the seismic nucleation phase.* Tectonophysics, **261**, 209-227.

Biagi P.F., Castellana L., Maggipinto T., Loiacono D., Schiavulli L., Ligonzo T., Fiore M., Suciu E. and Ermini A.; 2009: *A pre seismic radio anomaly revealed in the area where the Abruzzo earthquake (M=6.3) occurred on 6 April 2009.* Nat. Hazards Earth Syst. Sci., **9**, 1551-1556.

Biagi P.F., Castellana L., Maggipinto T., Loiacono D., Schiavulli L., Ligonzo T., Fiore M., Suciu E. and Ermini A.; 2010: *Brief communication ``A pre seismic radio anomaly revealed in the area where the Abruzzo earthquake (M=6.3) occurred on 6 April 2009''.* Nat. Hazards Earth Syst. Sci., **10**, 215-216.

Chao K. and Peng Z.; 2009: *Temporal changes of seismic velocity and anisotropy in the shallow crust induced by the 1999 October 22 M6.4 Chia-Yi, Taiwan earthquake.* Geophys. J. Int., **179**, 1800-1816, doi: 10.1111/j.1365-246X.2009.04384.x.

Cirella A., Piatanesi A., Cocco M., Tinti E., Scognamiglio L., Michelini A., Lomax A. and Boschi E.; 2009: *Rupture history of the 2009 L'Aquila (Italy) earthquake from non-linear joint inversion of strong motion and GPS data*. Geophys. Res. Lett., **36**, L19304, doi: 10.1029/2009GL039795.

Crescentini L. and Amoruso, A.; 1996: *Improving the SOPRA DMDP2000 spectrometer by a Michelson interferometer.* Rev. Sci. Instrum., **67**, 3044-3046.

Crescentini L. and Renzella G.; 1991: *A wide-band high-sensitivity laser strainmeter.* Rev. Sci. Instrum., **62**, 1206-1209.

Crescentini L., Amoruso A., Fiocco G. and Visconti G.; 1997*: Installation of a high-sensitivity laser strainmeter in a tunnel in central Italy.* Rev. Sci. Instrum., **68**, 887-905.

Dieterich J.H. and Kilgore B.; 1996: *Implications of fault constitutive properties for earthquake prediction.* Proc. Natl. Acad. Sci. U.S.A., **93**, 3787-3794.

Di Luccio F., Ventura G., Di Giovambattista R., Piscini A. and Cinti F.R.; 2010: *Normal faults and thrusts re-activated by deep fluids: the 6 April 2009 Mw 6.3 L'Aquila earthquake, central Italy.* J. Geophys. Res., **115**, B06315, doi: 10.1029/2009JB007190.

Dobrovolsky I.P., Zubkov S.I. and Miachin V.I.; 1979: *Estimation of the size of the earthquake preparation zones.* Pure Appl. Geophys., **117**, 1025-1044.

Dodge D.A., Beroza G.C. and Ellsworth W.L.; 1996: *Detailed observations of California foreshock sequences: Implications for the earthquake initiation process.* J. Geophys. Res., **101**, 22371-22392.

Einarsson P., Theodorsson P., Hjartardottir A.R. and Gujonsson G.I.; 2008: *Radon changes associated with the earthquake sequence in June 2000 in the south Iceland seismic zone.* Pure Appl. Geophys., **165**, 63-74, doi: 10.1007/s00024-007-0292-6.

Fang Z., Dieterich J.H. and Xu G.; 2010: *Effect of initial conditions and loading path on earthquake nucleation.* J. Geophys. Res., **115**, B06313, doi: 10.1029/2009JB006558.

Ghosh D., Deb A. and Sengupta R.; 2009: *Anomalous radon emission as precursor of earthquake.* J. Appl. Geophys., **69**, 67-81, doi: 10.1016/j.jappgeo.2009.06.001.

Giuliani G.G., Giuliani R., Totani G., Eusani G. and Totani F.; 2009: *Radon observations by Gamma Detectors "PM-4 and PM-2" during the seismic period (January – April 2009) in L'Aquila Basin.* Eos Trans. AGU, **90** (52), Fall Meet. Suppl., Abstract U14A-03.

Harris R.A. and Arrowsmith J.R.; 2006: *Introduction to the Special Issue on the 2004 Parkfield Earthquake and the Parkfield Earthquake Prediction Experiment.* Bull. Seismol. Soc. Am., **96**, S1-S10.

Inouchi N. and Sato H.; 1979: *Crustal deformation related to the Izu-Oshima Kinkai earthquake of 1978.* Bull. Geographical Surv. Inst., **23**, 14-24.

Johnston M.J.S. and Linde A.T.; 2002: *Implications of crustal strain during conventional, slow and silent earthquakes.* In: International Handbook of Earthquake and Engineering Seismology, Vol. 81A, Academic Press, New York, pp. 589-605.

Johnston M.J.S., Borcherdt R.D., Linde A.T. and Gladwin M.T.; 2006: *Continuous borehole strain and pore pressure in the near field of the 28 September 2004 M 6.0 Parkfield, California, earthquake: implications for nucleation, fault response, earthquake prediction, and tremor.* Bull. Seismol. Soc. Am., **96**, S56-S72.

Kanamori H.; 2003: *Earthquake prediction: an overview.* In: Lee W.H.K., Kanamori H., Jennings P. and Kisslinger C. (eds), International Handbook of Earthquake and Engineering Seismology, Part B, Academic Press, San Diego, pp. 1205-1216.

Kaneko Y. and Lapusta N.; 2008: *Variability of earthquake nucleation in continuum models of rate-and-state faults and implications for aftershock rates.* J. Geophys. Res., 113, B12312, doi: 10.1029/2007JB005154.

Kerr R.A.; 2009: *After the quake, in search of the science-or even a good prediction.* Science, **324**, 322.

Laubenstein M. and Magaldi D.; 2008: *Natural radioactivity of some red Mediterranean soils*. **Catena,** 76, 22-26.

Le Ravalec M., Gueguen Y. and Chelidze T.; 1996: *Magnitude of velocity anomalies prior to earthquakes*. J. Geophys. Res., **101**, 11217-11223.

Linde A.T., Gladwin M.T. and Johnston M.J.S.; 1992: *The Loma Prieta earthquake, 1989 and Earth strain tidal amplitudes: an unsuccessful search for associated changes*. Geophys. Res. Lett., **19**, 317-320.

Lisi M., Filizzola C., Genzano N., Grimaldi C.S.L., Lacava T., Marchese F., Mazzeo G., Pergola N. and Tramutoli V.; 2010: *A study on the Abruzzo 6 April 2009 earthquake by applying the RST approach to 15 years of AVHRR TIR observations.* Nat. Hazards Earth Syst. Sci., **10**, 395-406.

Lockner D.A.; 1998: *A generalized law for brittle deformation of Westerly granite.* J. Geophys. Res., **103**, 5107-5124.

Merino E. and Banerjee A.; 2008: *Terra Rossa genesis, implications for Karst, and Eolian dust: a geodynamic thread.* J. Geol., **116**, 62-75.

Mindlin R. D.; 1936: *Force at a point in the interior of a semi-infinite solid.* Physics, **7,** 195-202.

Nishimura E.; 1950: *On Earth tides*. Trans. Am. Geophys. Union, 31, 357-376.

Nur A.; 1972: *Dilatancy, pore fluids and premonitory variations of t_s/t_p travel times.* Bull. Seismol. Soc. Am., **62**, 1217-1222.

Pagiatakis S.D.; 1999: *Stochastic significance of peaks in the least-squares spectrum.* J. Geod., **73**, 67-78.

Park J., Amoruso A., Crescentini L. and Boschi E.; 2008: *Long-period toroidal earth free oscillations from the great Sumatra-Andaman earthquake observed by paired laser extensometers in Gran Sasso, Italy.* Geophys. J. Int., **173**, 887-905.

Plastino W., Nisi S., De Luca G., Balata M., Laubenstein M. and Bella F.; 2009: *Environmental radioactivity in the ground water at the Gran Sasso National Laboratory (Italy): a possible contribution to the variation of the neutron flux background.* J. Radioanal. Nucl. Chem., **282**, 809-813, doi: 10.1007/s10967-009-0151-2.

Plastino W., Povinec P.P., De Luca G., Doglioni C., Nisi S., Ioannucci L., Balata M., Laubenstein M., Bella F. and Coccia E.; 2010: *Uranium groundwater anomalies and L'Aquila earthquake, 6th April 2009 (Italy).* J. Environ. Radioact., **101**, 4550, doi: 10.1016/j.jenvrad.2009.08.009.

Rice J.R. and Rudnicki J.W.; 1979: E*arthquake precursory effects due to pore fluid stabilization of a weakened fault zone.* J. Geophys. Res., **84**, 2177-2184.

Roeloffs E.A.; 2006: *Evidence for aseismic deformation rate changes prior to earthquakes*. Annu. Rev. Earth Planet. Sci., **34**, 591-627.

Scholz C.H.; 1988: *The critical slip distance for seismic faulting.* Nature, **336**, 761-763.

Scholz C.H.; 2002: *The Mechanics of earthquake and faulting, 2nd ed.* Cambridge Univ. Press, Cambridge, 439 pp.

Scholz C.H., Sykes L.R. and Aggarwal Y.P.; 1973: *Earthquake prediction: a physical basis.* Science, **181**, 803-810.

Shaw B.E.; 2009: *Constant stress drop from small to great earthquakes in magnitude-area scaling*. Bull. Seismol. Soc. Am., **99**, 871-875, doi: 10.1785/0120080006.

Singh S., Kumar A., Singh Bajwa B., Mahajan S., Kumar V. and Dhar S.; 2009: *Radon monitoring in soil gas and ground water for earthquake prediction studies in north west Himalayas, India.* Terr. Atmos. Ocean. Sci., doi: 10.3319/TAO.2009.07.17.01(TT)

Tamura Y. and Agnew D.C.; 2008: *Baytap08 User's Manual.* UC San Diego: Scripps Institution of Oceanography. Retrieved from: http://escholarship.org/uc/item/4c27740c.

Venedikov A.P., Arnoso J. and Vieira R.; 2005: *New version of program VAV for tidal data processing.* Comput. Geosci., **31**, 667-669.

Walters R.J., Elliott J.R., D'Agostino N., England P.C., Hunstad I., Jackson J.A., Parsons B., Phillips R.J. and Roberts G.; 2009: *The 2009 L'Aquila earthquake (central Italy): A source mechanism and implications for seismic hazard*.

Geophys. Res. Lett., **36**, L17312, doi: 10.1029/2009GL039337.

Wyatt F.K., Agnew D.C. and Gladwin M.; 1994: *Continuous measurements of crustal deformation for the 1992 Landers earthquake sequence.* Bull. Seismol. Soc. Am., **84**, 768-779.

Zhang Y., Jian J., Qian J., Chen J., He S., Zhang Y. and He P.; 2002: *The crustal micro-deformation anomaly and the credible precursor.* Acta Seismol. Sin., **15,** 113-118.

Corresponding author: Antonella Amoruso
Dipartimento di Fisica, Università di Salerno
Via Ponte Don Melillo, 84084 Fisciano, Italy
Phone: +39 089 969129; fax: +39 089 969658 e-mail: antonella.amoruso@sa.infn.it